Title

Soil-gas Entry into Houses Driven by Atmospheric Pressure Fluctuations, Part 1 --- Measurements, Spectral Analysis, and Model Comparison

Journal

Atmospheric Environment, 31(10)

Author

Robinson, A.L.

Publication Date

1996-02-01

LBL-38232
UC-402
Preprint

Lawrence Berkeley Laboratory

UNIVERSITY OF CALIFORNIA

ENERGY & ENVIRONMENT DIVISION

Submitted to Atmospheric Environment

Soil-Gas Entry into Houses Driven by Atmospheric Pressure Fluctuations, Part 1—Measurements, Spectral Analysis, and Model Comparison

A.L. Robinson, R.G. Sextro, and W.J. Fisk

February 1996

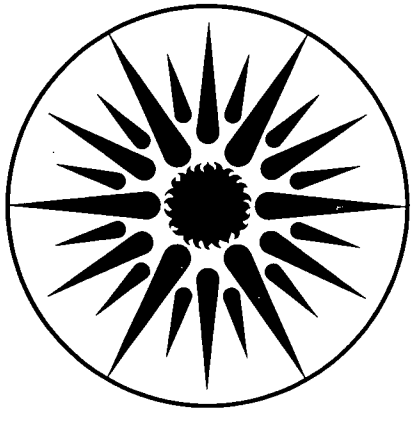

ENERGY AND ENVIRONMENT DIVISION

Prepared for the U.S. Department of Energy under Contract Number DE-AC03-76SF00098

DISCLAIMER

Submitted to *Atmospheric Environment*

LBL-38232
UC-402

Soil-Gas Entry into Houses Driven by Atmospheric Pressure Fluctuations, Part 1 --- Measurements, Spectral Analysis, and Model Comparison

Allen L. Robinson, Richard G. Sextro, William J. Fisk

February 1996

Indoor Environment Program
Energy and Environment Division
Lawrence Berkeley National Laboratory
1 Cyclotron Road
Berkeley, CA 94720

This work was supported by the Director, Office of Energy Research, Office of Health and Environmental Research, Environmental Sciences Division, and by the Assistant Secretary for Energy Efficiency and Renewable Energy, Office of Building Technology of the U.S. Department of Energy (DOE), under Contract DE-AC03-76SF00098.

ABSTRACT

To study the effect of atmospheric pressure fluctuations on the entry of radon and soil-gas contaminants into houses, we have simultaneously measured the gas flow rate into and out of an experimental basement structure and the changes in atmospheric pressure. Falling atmospheric pressure draws soil gas into the structure; rising atmospheric pressure drives air from inside the structure into the soil. The gas flow rate into and out of the structure depends on both the characteristic response time of the soil gas and the time-rate-of-change of an atmospheric pressure fluctuation. The larger the time-rate-of-change of a fluctuation in atmospheric pressure the larger the gas flow rate into the structure; a change in pressure must be sustained for a period comparable to several characteristic response times to maximize the soil-gas flow rate. Spectral analysis reveals that diurnal and semi-diurnal oscillations in atmospheric pressure drive the largest components of the long-term gas flow rate into and out of the structure. Analytical and numerical model predictions are compared to the detailed measurements of gas flow in both the time and frequency domains. The finite-element model correctly predicts both the dynamics and the magnitude of the observed gas flow, while the analytical model correctly predicts its dynamics, but underpredicts the amplitude of the observed flow by a factor of ~ 2.3. Atmospheric pressure fluctuations may increase the long-term radon entry rate into the experimental structure by as much as 0.2 Bq s^{-1}, more than twice the total diffusive entry rate.

Key word index: radon, atmospheric pressure, indoor-air quality, contaminant transport, soil-gas transport

INTRODUCTION

Recent theoretical (Narasimhan *et al.*, 1990; Tsang and Narasimhan, 1992) and experimental (Robinson and Sextro, 1995a) studies have shown that atmospheric pressure fluctuations can draw soil gas into houses. We are interested in the different mechanisms which induce soil-gas flow because the advective entry of radon-bearing soil gas into houses is generally believed to be the dominant transport mechanism of radon into most homes with elevated indoor concentrations (see e.g. review by Nazaroff (1992)). Advective soil-gas flow may also transport VOCs (volatile organic chemicals) from contaminated soils into buildings thereby contributing to indoor exposures to these contaminants (Wood and Porter, 1987; Hodgson *et al.*, 1992; Little *et al.*, 1992).

Soil-gas entry into houses is commonly associated with small but sustained indoor-outdoor pressure differences created by temperature effects, wind interaction with the building shell, and the operation of heating, ventilation and air-conditioning (HVAC) systems (Nazaroff *et al.*, 1988). The phrase "indoor-outdoor pressure difference" refers to the pressure difference between the ambient atmosphere at the soil surface and the indoor air at the mouth of an opening between the basement and the soil. Several field studies (Hernandez *et al.*, 1984; Holub *et al.*, 1985; Turk *et al.*, 1989; Hintenlang and Al-Ahmady, 1992) have observed elevated indoor radon concentrations during periods when indoor-outdoor pressure differences were apparently small. Atmospheric pressure fluctuations can draw soil gas into a house *without* these pressure differences because the response time of the interior of a house to a change in atmospheric pressure is generally several orders of magnitude shorter than the response time of the soil gas (Robinson and Sextro, 1995a). Consequently, soil-gas entry driven by atmospheric pressure fluctuations represents a possible explanation for these observed but unexplained elevated indoor radon concentrations.

The reported experimental evidence for radon entry driven by atmospheric pressure fluctuations is based on the correlation of atmospheric pressure with measured indoor radon concentrations (Hernandez *et al.*, 1984; Hintenlang and Al-Ahmady, 1992). Unfortunately, such studies provide little detailed insight into the effect of atmospheric pressure fluctuations on radon entry because indoor radon concentrations depend on both the entry rate and the building ventilation rate. Using a numerical model Tsang and Narasimhan (1992) have investigated the effect of periodic atmospheric pressure oscillations on radon entry. Although their results suggest that such oscillations may drive significant radon entry into houses for certain combinations of soil properties, basement configurations and atmospheric pressure signals, their efforts yield little physical insight into the phenomenon.

In this two part study, we present a detailed examination of the gas flow between a building and the underlying soil in response to changes in atmospheric pressure. The goal of this study is to characterize the relationship between this flow, soil properties, and typical atmospheric pressure fluctuations. A thorough understanding of this transient gas flow is an important step towards understanding the complex effect of atmospheric pressure fluctuations on the entry of radon and other soil-gas contaminants into buildings.

In this paper, we report measurements of gas flow and atmospheric pressure made in an experimental basement structure. We compare these measurements to predictions of both a finite-element and an analytical model. We

employ spectral analysis to examine our measurements and to validate the predictions of these models. In the second part of this study (Robinson *et al.*, 1996), these models are used to examine the sensitivity of the soil-gas entry into a house to changes in soil properties, water table depth, and the addition of a high-permeability gravel layer. Preliminary results of this investigation have been reported earlier (Robinson and Sextro, 1995a).

EXPERIMENTAL AND COMPUTATIONAL METHODS

Experimental System

The measurements reported in this study were made in an experimental structure which was designed and constructed to study soil-gas and radon entry into houses (Fisk *et al.*, 1992; Garbesi *et al.*, 1993; Robinson and Sextro, 1995b). Fig. 1 shows a schematic of the soil-structure system. The concrete structure is a single-chamber with interior dimensions of 2.0 x 3.2 m and a height of 2.0 m; only about 0.1 m of the walls extend above grade. The structure's floor slab rests on a 0.1-m-thick, high-permeability gravel layer. Two 1.25-cm-diameter holes in one wall of the access hatch permitted the interior of the structure to rapidly respond to changes in atmospheric pressure. A companion structure exists at this experimental site which is essentially identical to the one used for this study except that its floor slab rests on undisturbed soil.

The atmospheric pressure was measured at 0.2 Hz using a pressure transducer connected to an outdoor omnidirectional static pressure tap located ~ 3 m from the structure. The response time, accuracy, and resolution of this pressure transducer (Paroscientific model 1015a) are 1 s, ± 5 Pa, and 0.1 Pa, respectively. The pressure difference between the interior of the structure and the static pressure tap was measured at 30-s intervals using a differential pressure transducer (Validyne model DP103). We refer to this pressure difference as the indoor-outdoor pressure difference.

All openings between the structure interior and the soil are sealed except for a 3.8-cm-diameter hole in the center of the structure floor. Although this hole is not geometrically representative of the cracks and gaps which commonly exist in real houses (Scott, 1988), these experiments require such an opening in combination with a high-permeability subslab gravel layer to enable atmospheric pressure fluctuations to generate gas velocities greater than the detection limit of our flow sensor. Because of the high permeability of the subslab gravel layer, the soil-gas flow rate into the structure only weakly depends on the geometry of an opening if the opening does not provide significant resistance to flow. The effect of a gravel layer on steady-state soil-gas entry was examined by Robinson and Sextro (1996); its effect on transient entry is explored in the second part of this study (Robinson and Sextro, 1995b). Therefore, the measured gas flow rate through the hole is representative of the flow between the structure and the soil for more realistic opening configurations.

The gas flow rate through the 3.8-cm-diameter hole was measured using the flow sensor shown in Fig. 1. The 80-cm high sensor incorporates two omnidirectional hot-film velocity transducers (TSI model 8470) mounted in a U-shaped tube (1.9-cm ID) and measures the magnitude and direction of gas flow as small as 0.15 L min^{-1}. Two

velocity transducers are required to determine the direction of the soil-gas flow. A hot-film velocity transducer determines the gas velocity by measuring the heat loss rate from a small sphere which is maintained at a constant temperature difference above the surrounding gas. At low velocities (low gas flow rates), the complex interaction between the slight flow induced by this temperature difference and the mean gas flow around the sphere causes this heat loss rate to depend on the orientation of the gas velocity with respect to gravity (Hatton *et al.*, 1970). This effect enables us to determine the direction of the flow. At the same flow rate, the upward velocity reported by one transducer will be greater than the downward velocity reported by the other transducer. Although at flow rates in the sensor greater than 1 L min^{-1} this effect disappears, we assume that our sampling frequency of 0.2 Hz is much more rapid than the changes in flow direction, allowing us to record the direction of the lower velocities that accompany these changes. Because of the small size of the spherical sensing element, the slight flow induced by its elevated temperature does not affect our measurements of gas flow. The sensor was calibrated with a bubble flow meter. The response time, accuracy, and resolution of the flow sensor are 2 s, 5% of reading, and 0.02 L min^{-1} respectively. For the range of flows considered in this study, the resistance of the flow sensor tube varies linearly with flow and was measured in the laboratory to be 0.3 Pa L^{-1} min.

Measured Soil Properties

Table 1 reports the measured permeability of the gravel, backfill, and undisturbed soil at the structure site. The permeability of the undisturbed soil is scale dependent, increasing by more than an order of magnitude when the measurement scale increases from 0.1 to 3.5 m (Garbesi *et al.*, 1995). In Table 1 we report the values measured at the 3.5-m scale, the longest length scale at which measurements were made. Although the length scale of our system is ~ 6.5 m (defined by the depth of the water table below the structure floor slab), the measurements suggest that the horizontal permeability of the undisturbed soil approaches an asymptote of ~ 3 x 10^{-11} m^2 at length scales greater than 3 m (Garbesi *et al.*, 1995). The backfill region, shown in Fig. 2, was excavated during the construction of the structure. It was carefully refilled to minimize the disturbance of the native soil environment (Fisk *et al.*, 1992). The careful packing of the backfill region is thought to have destroyed the features which create the scale dependence observed in the undisturbed soil.

Measurements of the air-filled porosity of the soil at the structure site are summarized in Table 2. We calculated this porosity profile based on gravimetric analysis (Danielson and Sutherland, 1986) of soil cores taken by Flexser et al (1993). The change in porosity between 1.6 and 2.2 m corresponds to the transition between the organic surface soil and the underlying sapprolite. Further geological details of the structure site are described by Flexser *et al.* (1993) and Brimhall and Lewis (1992).

Spectral Analysis of Experimental Data

Data for spectral analysis were collected over a period of 30 days in the fall of 1994. This data set is continuous except for four ~ 1 hr periods during which data were downloaded. For this analysis, the data were broken into overlapping, equal length time blocks (Bendat and Piersol, 1986). To eliminate the influence of soil-gas flow driven

by indoor-outdoor pressure differences on our estimates, time blocks were discarded in which the measured indoor-outdoor pressure differences were greater or less than +/- 0.5 Pa. These periods occurred during storms when high winds (speeds greater than ~5 m s^{-1}) blowing over the open holes in the structure access hatch depressurized the interior of the structure relative to the outside. The application of this criterion resulted in data being drawn from approximately 21 non-sequential days of the measurements.

We employ the algorithms described by Bendat and Piersol (1986) to estimate: 1) the atmospheric pressure, time-rate-of-change of atmospheric pressure, and soil-gas flow rate power spectra, and 2) the gain and phase functions of the soil-structure system. Briefly, the Hanning taper window (Bendat and Piersol, 1986) was applied to the data in each time block to reduce leakage of power to adjacent frequency bins. The data were then transformed into the frequency domain using a fast Fourier transform. The Fourier transforms of the data within each time block were corrected for power loss due to the taper window, and then averaged to generate smooth, consistent spectral estimates of the various power spectra and gain and phase functions using the expressions described by Bendat and Piersol (1986). To minimize the effect of aliasing on our estimates, the highest 25% of the frequency ordinates of each periodogram were discarded.

We analyzed the reduced data set twice using different length time blocks. To increase the resolution of our estimates at low frequencies, 5-day-long blocks were used to calculate the various spectral functions at frequencies less than 200 day^{-1}. To decrease the variance of our estimates at higher frequencies, 24-hour-long blocks were used to estimate these functions at frequencies greater than 100 day^{-1}. These estimates were combined by averaging their values in overlapping frequency bins.

Theoretical Framework for Predicting Transient Soil-gas Flow

In this section we describe the equations which govern the transient flow of soil gas into houses. In subsequent sections we describe both an analytical and numerical model which we use to solve these equations and predict the gas flow rate into and out of the experimental structure in response to changes in atmospheric pressure

Combining Darcy's law and the continuity equation, and considering soil air as a compressible ideal gas, the equation which predicts the propagation of a pressure fluctuation through a porous medium is (see e.g. (Massmann, 1989))

$$\frac{\partial p}{\partial t} = \frac{k}{\varepsilon \mu} \nabla (p \nabla p) \qquad (1)$$

where p is the soil-gas pressure (Pa), k is the soil permeability to air (m^2), ε is the air-filled porosity (-), and μ is the dynamic viscosity of the soil gas (Pa s). Massmann (1989) shows that for small deviations from the mean pressure (< 5 %), eqn. (1) can be approximated with negligible error by the linear transient diffusion equation

$$\frac{\partial p}{\partial t} = D_p \nabla^2 p \qquad \text{where} \quad D_p = \frac{k \bar{P}}{\mu \varepsilon} \qquad (2)$$

where D_p is the pressure diffusivity ($m^2\ s^{-1}$), and $\bar{P}$ is the mean soil-gas pressure (Pa). Many authors (e.g. Buckingham, 1904; Fukuda, 1955; Weeks, 1979) have used the transient diffusion equation to predict soil gas response to atmospheric pressure fluctuations. After eqn. (1) or (2) has been solved, the soil-gas velocity field, $\bar{v}$ (m s^{-1}), can be calculated with Darcy's law,

$$\bar{v} = \frac{-k}{\mu} \nabla p \tag{3}$$

Utilizing dimensional analysis, we can estimate a characteristic response time of the soil gas to a change in pressure. Such a response time, τ (s), can be derived from eqn. (2),

$$\tau = \frac{L^2}{D_p} \tag{4}$$

where L is the characteristic length scale of the system (m). Physically, τ characterizes the time for a pressure perturbation to propagate the distance L.

Since the equation which predicts the propagation of small pressure perturbations through a porous medium is linear, many powerful analysis tools can be used to investigate soil-gas flow driven by changes in atmospheric pressure. This transient flow can be equivalently characterized in both the time and the frequency domains (Chatfield, 1989). There are many advantages to examining this flow in the frequency domain because typical atmospheric pressure signals are dominated by large oscillations at two or three frequencies (Gossard, 1960). Several studies (Burkhard *et al.*, 1987; Nilson *et al.*, 1991; Neeper and Limback, 1994) have employed spectral techniques to analyze soil-atmosphere interactions.

In the time domain, the transient response of the soil gas to changes in atmospheric pressure is characterized in terms of the step-response function. The step-response function defines the soil-gas flow rate into the structure caused by a unit-step change in atmospheric pressure. Once this function is known, the soil-gas flow rate caused by *any* change in atmospheric pressure can be determined by convoluting the step-response function with the atmospheric pressure signal. In the study of heat conduction this convolution is known as Duhamel's theorem (Carslaw and Jaeger, 1959). Duhamel's theorem states that the soil-gas flow rate can be expressed in terms of either atmospheric pressure or the time-rate-of-change of atmospheric pressure. We will develop both formulations to compare and contrast these two ways at looking at the problem. Duhamel's theorem defines the gas flow rate into and out of the structure in response to changes in atmospheric pressure, q(t) ($m^3\ s^{-1}$), as

$$q(t) = \int_{-\infty}^{t} Q_{step}(t-\theta)\, P'_{atm}(\theta) d\theta, \text{ or} \tag{5a}$$

$$q(t) = \int_{-\infty}^{t} Q'_{step}(t-\theta)\, P_{atm}(\theta) d\theta \tag{5b}$$

where Q_{step} is the step-response function of the soil-structure system ($m^3\ s^{-1}\ Pa^{-1}$), Q'_{step} is the time derivative of the

step-response function ($m^3\ s^{-2}\ Pa^{-1}$), P_{atm} is the atmospheric pressure (Pa), P'_{atm} is the time-rate-of-change of atmospheric pressure ($Pa\ s^{-1}$), and θ is a dummy variable indicating integration over time (s).

In the frequency domain, the transient response of the soil gas to changes in atmospheric pressure is characterized by the frequency response function. The frequency response function defines the amplitude and the phase of the soil-gas flow rate caused by a sinusoidal oscillation in atmospheric pressure. Because the equation which governs the propagation of a pressure perturbation through a porous medium is linear, a sinusoidal oscillation in atmospheric pressure will drive a sinusoidal oscillation of soil-gas flow at the *same* frequency (Chatfield, 1989). The frequency response function can be defined as the Fourier transform of the step-response function:

$$\chi(\omega) = \int_0^\infty Q_{step}(\theta)\exp(-i\omega\theta)d\theta, \text{ or} \tag{6a}$$

$$d\chi(\omega) = \int_0^\infty Q'_{step}(\theta)\exp(-i\omega\theta)d\theta \tag{6b}$$

where $i = \sqrt{-1}$, and ω is the circular frequency (radians s^{-1}).

We will report the complex valued frequency response function in terms of the gain, $G(\omega)$, and phase, $\phi(\omega)$, functions (Chatfield, 1989),

$$G_{q,dp}(\omega) = |\chi(\omega)| \quad \text{and} \quad \phi_{q,dp}(\omega) = \arg(\chi(\omega)) \tag{7a}$$

$$G_{q,p}(\omega) = |d\chi(\omega)| \quad \text{and} \quad \phi_{q,p}(\omega) = \arg(d\chi(\omega)) \tag{7b}$$

where $|\ |$ and arg( ) indicate the magnitude and argument of a complex number. $G_{q,dp}(\omega)$ ($m^3\ Pa^{-1}$) and $\phi_{q,dp}(\omega)$ (radians) define the amplitude and phase of the soil-gas flow rate caused by an oscillation in the time-rate-of-change of atmospheric pressure as a function of frequency. $G_{q,p}(\omega)$ ($m^3\ s^{-1}\ Pa^{-1}$) and $\phi_{q,p}(\omega)$ (radians) define the amplitude and phase of the soil-gas flow rate caused by a oscillation of atmospheric pressure as a function of frequency.

Description of the Analytical Model

In this section we derive analytical expressions for the step and frequency response functions of the experimental structure based on an exact solution of eqn. (2). The model predicts the soil-gas flow underneath the structure by approximating this flow as one-dimensional in the vertical plane between the deep soil and the gravel layer. The flow underneath the structure is approximated as one-dimensional because: 1) the gravel layer acts as an isobaric plenum (Robinson and Sextro, 1995b), and 2) atmospheric pressure fluctuations drive flow because of the compressibility of the soil gas. Although the flow within the gravel layer is not one-dimensional because of the convergence of the flow field into the hole in the concrete floor slab, we have assumed that this does not significantly affect the flow rate into the basement because the permeability of a gravel layer is almost 3 orders of magnitude larger than the permeability of the undisturbed soil. The analytical model assumes that the pressure within the gravel

compressibility of the soil gas. Although the flow within the gravel layer is not one-dimensional because of the convergence of the flow field into the hole in the concrete floor slab, we have assumed that this does not significantly affect the flow rate into the basement because the permeability of a gravel layer is almost 3 orders of magnitude larger than the permeability of the undisturbed soil. The analytical model assumes that the pressure within the gravel layer is uniform, and that the gas flow rate into and out of the structure is equal to the flow between the soil and the gravel layer.

With these assumptions, the step-response function of the soil-structure system can be approximated by solving eqn. (2) with the following initial and boundary conditions: initial condition, p(z,0) = 0 Pa; boundary condition #1, p(0,t) = 1 Pa (unit step change in pressure in the gravel layer defined at z = 0); boundary condition #2 $\partial p(L,t)/\partial z$ = 0 (a no flow boundary at the z = L; physically this boundary represents a water table, bedrock, or some other impermeable layer). The analytical model defines the interface between the gravel layer and the soil as z = 0. Assuming homogeneous soil, the solution of eqn. (2) for these boundary conditions is (Carslaw and Jaeger, 1959)

$$p(z,t) = -\frac{4}{\pi}\sum_{n=0}^{\infty}\frac{\sin\left[(2n+1)\frac{\pi}{2}\frac{z}{L}\right]}{(2n+1)}\exp\left[\frac{-t}{T_n}\right] \qquad \text{defined for } t \geq 0 \qquad (8)$$

where $T_n = \frac{1}{(2n+1)^2}\left(\frac{4}{\pi^2}\right)\left(\frac{L^2}{D_p}\right)$ (s). Using eqns. (3) and (8) and our assumption that the gas flow rate into the structure is equivalent to the soil-gas flow into the gravel layer, we can write the structure's step-response function as

$$Q_{step}(t) = \frac{k}{\mu}\frac{2}{L}A\sum_{n=0}^{\infty}\exp\left(\frac{-t}{T_n}\right) \qquad \text{defined for } t \geq 0 \qquad (9)$$

where A is the vertical cross-sectional area of the gravel layer (m^2). Using eqns. (6a) and (9) we can derive an expression for the frequency response function defined by the analytical model, $\chi_a(\omega)$,

$$\chi_a(\omega) = \frac{k}{\mu}\frac{8}{\pi^2}\frac{L}{D_p}A\sum_{n=0}^{\infty}\left(\frac{1}{(2n+1)^2}\right)\left(\frac{1-i\omega T_n}{1+(\omega T_n)^2}\right) \qquad \text{defined for } \omega > 0. \qquad (10)$$

Eqns. (8)-(10) indicate that computation of the analytical model requires the evaluation of an infinite series. Fortunately, this series rapidly converges and only a limited number of terms need be considered to accurately approximate the analytical solution. We considered the series converged when the relative error of neglecting an additional term was less than 10^{-8}. Values of the different soil and geometric properties used as inputs for the analytical model to simulate gas flow into and out of the experimental structure are listed in Table 3. Because the analytical model assumes a homogeneous soil, the values for permeability and air-filled porosity listed in Table 3 are averages of measurements. The measured values of these soil properties are summarized in Tables 1 and 2.

Description of Numerical Simulations

A transient, finite-element model was used to predict the gas flow rate into and out of the experimental basement structure. The model calculates this flow rate by solving eqns. (1) and (3) over the region shown in Fig. 2. The gas flow rate into and out of the structure is defined by the soil-gas velocity normal to the opening in the basement floor. The code is a modified version of the RN3D model written by Holford (1994). RN3D was developed to simulate gas flow and radon transport in variably saturated, non-isothermal porous media. The original code only simulates regularly shaped geometries; we have written a preprocessor to generate a two-dimensional mesh with an irregularly shaped boundary required for simulating soil-gas flow around a basement. Holford (1994) describes the mathematics, numerics, and physics of the model.

Although the experimental structure has a rectangular floor plan, we simulated it as a cylindrical basement surrounded by a cylindrical soil block. The radius of the simulated gravel layer was defined to match the vertical cross-sectional area of the gravel layer of the real structure, 5 m^2. By simplifying the problem into an axial-symmetric radial coordinate system we significantly reduce the computational requirements of the model while preserving the structure volume and floor area. In addition, by utilizing a cylindrical coordinate system we can accurately simulate the convergence of the soil-gas flow field into the hole in the center of the structure floor. We divided the model's soil block into the three regions shown in Fig. 2. The permeability values assigned to each region are listed in Table 1. The air-filled porosity of the soil block varied with depth as summarized in Table 2.

To examine the gas flow rate into and out of the structure driven by atmospheric pressure fluctuations, we used the finite-element to simulate the step-response function. For this simulation the following initial and boundary conditions are used: initially ($t = 0$ s) the entire soil block was assigned a pressure of 92,200 Pa (the average atmospheric pressure measured at the experimental site); for $t > 0$ s the soil surface (indicated as P1 in Fig. 2) and the mouth of the hole (indicated as P2 in Fig. 2) were assigned a pressure of 92,199 Pa. As Fig. 2 indicates, the outside edge of the structure's concrete walls, floor, and footer are defined as no flow boundaries. The bottom of the soil block is defined as a no flow boundary at the measured depth of the water table. The outside edge of the soil block is also defined as a no flow boundary. The radius of the soil block (15 m) was chosen such that outside edge of the soil block falls outside the domain of influence of the structure.

To simulate the step-response function, the finite-element model marches forward in time utilizing a fully-implicit time-discretization scheme until the soil-gas flow rate into the structure had fallen 7 orders of magnitude from its peak value. At this point, we assume that the soil gas and atmospheric pressure have reached equilibrium and the simulation is ended. We assumed that the atmospheric pressure is uniform across the entire surface of the soil, and that changes in atmospheric pressure are communicated instantaneously to the interior of the structure.

After determining the step-response function, we calculated the gain and phase functions by first numerically evaluating eqn. (5a) and then applying the definitions shown in eqns. (7a) and (7b). The gas flow rate into and out of the structure in response to different atmospheric pressure signals was determined by numerically evaluating eqn (5a). By indirectly calculating this flow using the step-response function, the computational time to simulate a

particular atmospheric pressure signal is reduced by several orders of magnitude in comparison to directly simulating that pressure signal with the finite-element model. To examine the difference between the soil-gas flow rate calculated using the step-response function and the flow rate calculated directly by the finite-element model, we directly simulated 1 hr of atmospheric pressure data with the model. The maximum difference between the flow rate directly computed by the finite-element model and the flow rate calculated using the step-response function was less than 0.04 L min^{-1}, yielding an average relative error of less than 0.5%.

An iterative procedure was used to incorporate the resistance of the flow sensor in the simulations. For each time step the pressure at the mouth of the hole was initially set equal to the pressure in the basement. The model then calculated the soil-gas flow rate into the basement. The pressure boundary condition at the bottom of the opening was adjusted to account for the resistance of the flow sensor and the flow rate into the structure was recomputed. This procedure was repeated until the flow rate had converged, defined as a relative flow change of less than 10^{-4} between iterations.

We also employed the finite-element model to simulate soil-gas entry driven by a steady-state indoor-outdoor pressure difference. For these calculations, the model solves the steady-state form of eqn. (1) with the following boundary conditions: soil surface (indicated as P1 in Fig. 2) is assigned a pressure of 92,200 Pa, and mouth of the opening is assigned a pressure of 92,199 Pa. As previously described, all of the other boundaries of the soil block are defined as no-flow.

RESULTS AND DISCUSSION

Since most investigations of soil-gas entry into houses have focused on entry driven by indoor-outdoor pressure differences, we briefly compare this entry to entry caused by changes in atmospheric pressure before presenting our measurements of gas flow and atmospheric pressure. A comparison of the flow field around the experimental structure created by an indoor-outdoor pressure difference to one induced by a change in atmospheric pressure highlights many of the differences between these two phenomena.

We employed the finite-element model to illustrate the nature of these flow fields. Fig. 3a shows the calculated soil-gas pressure and velocity fields caused by a constant time-rate-of-change of atmospheric pressure. The streamlines indicate that a change in atmospheric pressure drives essentially one-dimensional flow between the deep soil and the gravel layer underneath the structure. For comparison, predictions of the soil-gas pressure and velocity fields caused by steady indoor-outdoor pressure difference are shown in Fig. 3b. An indoor-outdoor pressure difference creates a more complex, three-dimensional flow field because the driving potential for flow exists between the interior of the structure and surface of the soil.

Although the different mechanisms which create indoor-outdoor pressure differences vary in time (Nazaroff *et al.*, 1988), most analyses of soil-gas entry driven by these pressure differences assume that this entry can be approximated as a steady-state process in which the soil gas is treated as incompressible (see review by Nazaroff

(1992)). Thus, the flow of soil gas into a basement driven by indoor-outdoor pressure differences is balanced by flow from the atmosphere into the soil. In contrast, soil-gas flow driven by changes in atmospheric pressure is fundamentally a transient phenomena where atmospheric pressure fluctuations drive gas flow because of the compressibility of the soil gas. A change in atmospheric pressure causes a net gas flow either into or out of the soil as the soil gas adjusts to the new pressure.

Atmospheric Pressure and Soil-gas Entry Measurements in the Time Domain

In Fig. 4, measurements of atmospheric pressure made during a 6-day experiment indicate that atmospheric pressure fluctuations occur at a variety of amplitudes and time scales. Several mechanisms, ranging from the diurnal heating of the earth to turbulent wind fluctuations, create changes in atmospheric pressure (Gossard and Hooke, 1975). The response of the soil-structure system to changes in atmospheric pressure depends on the characteristic response time of the soil gas to changes in pressure. Using eqn. (4) and values for L and D_p listed in Table 3, the characteristic response time of our soil-gas to a change in surface pressure is ~ 2 min --- much shorter than the time scale of the large atmospheric pressure fluctuations shown in Fig. 4.

Measurements of atmospheric pressure and the gas flow rate into and out of the experimental structure for a 1-hr period of the 6-day experiment are presented in Fig. 5. This 1-hr period was chosen because the large soil-gas flows clearly illustrate the dynamics of the soil-atmosphere interaction. Fig. 5a shows atmospheric pressure oscillations with a period of ~20 min and an amplitude of ~10 Pa. The calculated time-rate-of-change in atmospheric pressure, approximated with a central difference, is shown in Fig. 5b. The measured gas flow rate into and out of the structure is shown in Fig. 5c. During this period, the average indoor-outdoor pressure difference was -0.02 Pa with a standard deviation of 0.25 Pa (approximately the resolution of the pressure transducer).

A comparison of the calculated time-rate-of-change of atmospheric pressure, shown in Fig. 5b, and the measured gas flow rate, shown in Fig. 5c, reveals that the soil-gas flow rate generally follows the time-rate-of-change of atmospheric pressure. Falling atmospheric pressure drives soil-gas entry into the structure; rising atmospheric pressure drives air from inside of the structure into the soil. The larger the time-rate-of-change of atmospheric pressure the larger the gas flow rate into or out of the structure. The soil-gas flow rate does not respond to the high frequency fluctuations in atmospheric pressure because the characteristic response time causes the soil to act as a high-frequency filter.

Model Predictions in the Time Domain

Predictions of the finite-element and the analytical model are compared to the measurements in Figs. 5c and 5d, respectively. The finite-element model correctly predicts both the amplitude and the dynamics of the gas flow rate into and out of the experimental structure for this one hour period. The analytical model correctly predicts the dynamics of the observed gas flow but underpredicts the magnitude of the entry by a factor of ~ 2.3.

The calculated soil-gas flow field shown in Fig. 3a suggests that the underprediction of the observed soil-gas flow rate by the analytical model may be due to its failure to account for the two-dimensional components of the flow

field underneath the structure. Because the floor of the structure lies 2-m below the soil surface changes in atmospheric pressure propagate both vertically and horizontally away from the gravel layer.

Measured Atmospheric Pressure and Soil-gas Entry Power Spectra

To illustrate the spectral composition of a typical atmospheric pressure signal and the long-term soil-gas flow rate, power spectra estimated from more than 21 days of measurements are presented in Fig. 6. The large peaks in the atmospheric pressure power spectrum, shown in Fig. 6a, correspond to ~150 Pa diurnal and semi-diurnal oscillations in atmospheric pressure such as those shown in Fig. 4. The absence of any significant high-frequency spikes indicates that large, high-frequency pressure oscillations such as those shown in Fig. 5a occur only intermittently. The spectrum shown in Fig. 6a is consistent with previously reported estimates of the atmospheric pressure power spectrum (Gossard, 1960).

The calculated soil-gas flow and time-rate-of-change power spectra are shown in Fig. 6b. A comparison of these spectra reveals that the power distributions for soil-gas flow and the time-rate-of-change in atmospheric pressure match. The peaks at frequencies of 1 and 2 day^{-1} indicate large diurnal and semi-diurnal oscillations in the soil-gas flow rate. Approximately 3% of the total power of the soil-gas flow spectrum corresponds to a diurnal oscillation, and ~ 10% corresponds to a semi-diurnal oscillation. More than 60% of the total power of the soil-gas flow spectrum occurs at frequencies less than 100 day^{-1}.

Measured Gain and Phase Functions

By transforming our analysis into the frequency domain we can gain valuable insight into soil-gas flow driven by atmospheric pressure fluctuations. In the frequency domain, the gain and phase functions define the soil-gas flow rate caused by any change in atmospheric pressure. The estimates of these functions shown in Fig. 7 were calculated from 21 days of atmospheric pressure and gas flow measurements.

The estimate of $G_{q,p}(\omega)$ shown in Fig. 7a indicates the amplitude of the soil-gas flow rate caused by a 1 Pa oscillation in atmospheric pressure as a function of frequency. The shape of $G_{q,p}(\omega)$ reveals that low-frequency oscillations in atmospheric pressure require large amplitudes to drive significant gas flow into and out of the structure. For example, a diurnal oscillation in atmospheric pressure with an amplitude of 1 Pa drives only a 0.001 L min^{-1} diurnal oscillation in gas flow into and out of the structure. In comparison, a 1 Pa 100 day^{-1} oscillation in atmospheric pressure drives a 0.1 L min^{-1} 100 day^{-1} oscillation in gas flow. This occurs because the time-rate-of-change of a sinusoid varies linearly with its frequency; consequently, low-frequency atmospheric pressure oscillations require very large amplitudes to generate significant time-rates-of-change. This behavior underscores the utility of thinking about this phenomenon in terms of the time-rate-of-change in atmospheric pressure.

The shape of $G_{q,dp}(\omega)$, shown in Fig. 7b, illustrates the relationship between soil-gas flow and the characteristic response time of the soil gas to a change in pressure. Physically, we can interpret $G_{q,dp}$ as the amplitude of the soil

gas flow caused by a 1 Pa min^{-1} oscillation in the time-rate-of-change of atmospheric pressure. The roll-off of $G_{q,dp}$ at a frequency of ~ 50 day^{-1} reveals that the soil acts as low pass filter. For a given amplitude, low-frequency oscillations in the time-rate-of-change atmospheric pressure will drive the largest soil-gas flow rates. The roll-off of $G_{q,dp}(\omega)$ occurs at the frequency at which the characteristic response time of the soil gas (τ ~ 2 min) limits the gas flow into and out of the structure.

The estimates of the phase functions shown in Fig. 7c further illustrate the relationship between the characteristic response time and the flow rate into and out of the structure. Physically, the phase function is the phase shift between the soil-gas flow rate and oscillations in atmospheric pressure. At frequencies less than 30 day^{-1}, $\phi_{q,dp}(\omega)$ indicates that the soil-gas flow rate and the time-rate-of-change are in phase --- the maximum soil-gas flow rate corresponds to the maximum time-rate-of-change of atmospheric pressure. As the frequency of the oscillations increases, the gas flow lags behind the time-rate-of-change of atmospheric pressure because of the finite response time of the soil gas.

The coherence of the measurements of gas flow and atmospheric pressure is shown in Fig. 8. The coherence indicates the linear correlation between the soil gas flow rate and the changes in atmospheric pressure as a function of frequency. The coherence varies between 0 and 1; the closer the coherence is to 1 the stronger the correlation (Chatfield, 1989). The coherence is greater than 0.85 for frequencies between 2 and 200 day^{-1} indicating a strong correlation between the observed gas flow and changes in atmospheric pressure. At very low frequencies, the coherence falls off because the frequency of the estimate approaches the spectral resolution of our analysis, ~ 0.17 day^{-1}. At high frequencies, we hypothesize that the coherence falls off because the size of both the atmospheric pressure and gas flow rate approach the resolution of our sensors. In addition, wind fluctuations may increase the experimental noise at these frequencies.

Comparison of Measured and Predicted Gain and Phase Functions

In Fig. 7, the gain and phase functions estimated from our measurements are compared to those predicted by both the analytical and numerical model. This comparison enables us to examine the predictions of these models over the entire range of possible atmospheric pressure fluctuations.

As expected from our analysis in the time domain, both models appear to correctly predict the dynamics of the observed soil-gas flow. Figs. 7a and 7b indicate that the finite-element model overpredicts by ~ 30% the magnitude of the gas flow rate driven by atmospheric pressure fluctuations with a frequency less than 100 day^{-1}. At frequencies greater than 100 day^{-1} the finite element model predicts the amplitude of the soil-gas flow rate to within 15%. Fig. 7a and 7b indicate that the analytical model underpredicts the amplitude of the observed gas flow rate by a factor of ~ 2.3 across the entire frequency band.

Comparing the measured and predicted phase functions in Fig. 7c indicates that both models correctly predict the phase lag between the soil-gas flow rate and oscillations in atmospheric pressure at frequencies less than

200 day^{-1}. However, the predicted and measured phase functions approach different high-frequency limits. We hypothesize that this discrepancy can be attributed to the magnitude of the high frequency changes in both the atmospheric pressure and the soil-gas entry rate approaching the resolution of our sensors. The coherence shown in Fig. 8 indicates that the correlation between the measured soil-gas entry rate and changes in atmospheric pressure falls off at high frequencies.

Considering the uncertainties associated with both our measurements of the gas flow rate and the soil properties used as inputs for the simulations, the predictions of the finite-element model are excellent. Our examination of the sensitivity of soil-gas flow to changes in soil properties presented in the second part of this study (Robinson *et al.*, 1996) suggests that the overprediction of the observed gas flow rate caused by low-frequency oscillations in atmospheric pressure by the finite-element model may be caused by the uncertainty in the air-filled porosity values used as inputs for the model. As Table 2 indicates, we assumed an air-filled porosity of 0.25 below 5.0 m; reducing the air-filled porosity in this region will decrease the gas flow into and out of the structure calculated by the finite-element model.

Contaminant Entry Driven by Atmospheric Pressure Fluctuations

Although the time-averaged gas flow between the soil and the interior of the structure driven by atmospheric pressure fluctuations is zero, these fluctuations can produce a net radon (or other soil-gas contaminant) entry rate because the radon concentration of the soil gas is generally orders of magnitude larger than indoor air. Unfortunately, detailed analysis of this entry is complicated by the dilution of the radon concentration of the soil gas immediately underneath the structure by "fresh" air flowing out of the ventilated structure in response to increases in atmospheric pressure.

By ignoring the effects of this dilution we can calculate an upper bound for the long-term radon entry rate caused by typical atmospheric pressure fluctuations. Atmospheric pressure fluctuations draw ~ 230 L of soil gas into the structure each day. Based on measurements made during steady-state radon entry experiments, the average radon concentration of the soil gas underneath the structure floor slab is ~ 90,000 Bq m^{-3} (Robinson and Sextro, 1995b). If the radon concentration of the soil gas underneath structure's floor slab was not diluted by the outflow of indoor air, atmospheric pressure fluctuations would increase the long-term radon entry rate into the structure by 0.2 Bq s^{-1}, more than twice the total measured diffusive entry rate into the structure. To compare this estimate with entry driven by steady indoor-outdoor pressure differences, we calculated an equivalent steady-state soil-gas entry rate. This equivalent steady-state entry rate is 0.15 L min^{-1} which corresponds to the entry rate caused by 0.4 Pa steady indoor-outdoor difference. Such a pressure difference is commonly found in real houses (Nazaroff, 1992).

CONCLUSIONS

Atmospheric pressure fluctuations can draw soil gas into buildings without the indoor-outdoor pressure differences commonly associated with the advective entry of radon and other soil-gas contaminants. Consequently,

atmospheric pressure fluctuations may represent an important mechanism for driving advective entry of radon and soil-gas contaminants into buildings.

The potential of an atmospheric pressure fluctuation for driving soil gas flow is determined by both its time-rate-of-change and the period over which it occurs. The larger the time-rate-of-change of an atmospheric pressure fluctuation the larger the soil-gas flow rate. However, changes in atmospheric pressure must be sustained to drive significant soil-gas flow. If a change is sustained for a period less than the characteristic response time of the soil gas to a change in pressure, this response time limits the flow rate into the structure --- effectively creating a low-pass filter. Changes in pressure must be sustained for a period comparable to several characteristic response times to maximize the soil-gas flow rate into or out of the structure.

Spectral analysis has revealed that diurnal and semi-diurnal oscillations in atmospheric pressure drive the largest component of the long-term gas flow rate into and out of the structure. These fluctuations are the most important because of their relatively large magnitude (~150 Pa) and their consistency. The largest observed soil-gas flow rates corresponded to relatively rapid (~20 min) and small (~15 Pa) fluctuations in atmospheric pressure. However, such high-frequency pressure oscillations only occur intermittently and therefore do not significantly contribute to the long-term gas flow rate.

A transient finite-element model based on Darcy's law with regionally defined soil properties correctly predicts the observed gas flow rates into and out of the experimental structure. An analytical model based on a one-dimensional solution of the diffusion equation correctly predicts the dynamics of the gas flow, but underpredicts its magnitude by a factor of ~2.3. We hypothesize that this underprediction may be caused by the failure of the analytical model to account for two-dimensional components of the soil-gas flow field underneath the experimental structure.

Soil-gas flow into houses driven by atmospheric pressure fluctuations is fundamentally different than entry driven by indoor-outdoor pressure differences. Indoor-outdoor pressure differences drive three-dimensional flow between the soil surface and openings in the building's substructure. In contrast, atmospheric pressure changes drive transient, largely one-dimensional flow between the basement and the deep soil. Because of these differences, we expect that the relationship between soil-gas entry, the properties of the soil, and the characteristics of a building's substructure will depend on whether this entry is driven atmospheric pressure fluctuations or indoor-outdoor pressure differences. In the second part of this study (Robinson *et al.*, 1996), we examine the influence of soil properties, water table depth, and a high-permeability subslab gravel layer on soil-gas entry.

Acknowledgments

The authors thank M. Fischer, R. Greif, W. Nazaroff, W. Riley, and S. Schery for their reviews of this manuscript and J. Li and Y. Tsang for suggesting this application of RN3D. We are also grateful to the California Department of Forestry and the Ben Lomond Nursery for their hospitality at the field site.

REFERENCES

Bendat J. S. and Piersol A. G. (1986) *Random data: analysis and measurement procedures*. Wiley-Interscience, New York.

Brimhall G. H. and Lewis C. J. (1992) Differential element transport in the soil profile at the Ben Lomond small structure radon site: A geochemical mass balance study. University of California at Berkeley, Dept. of Geology and Geophysics, Berkeley CA 94720.

Buckingham E. (1904) Contributions to our knowledge of the aeration of soils. *U.S. Dept. Agriculture Soils Bur. Bull.* **25**, 3-52.

Burkhard N. R., Hearst J. R. and Hanson J. M. (1987) Estimation of the bulk diffusivity of chimneys using post-shot holes. Proceeding of Fourth Symposium on Containment of Underground Nuclear Tests, Rep. LLNL-CONF-870961. Lawrence Livermore National Laboratory, Livermore CA 94550.

Carslaw H. S. and Jaeger J. C. (1959) *Conduction of Heat in Solids*. Clarendon Press, Oxford.

Chatfield C. (1989) *The analysis of time series: an introduction*. Chapman and Hall, London.

Danielson R. E. and Sutherland P. L. (1986) Porosity. In Black C. A. (Ed.) *Methods of soil analysis, part 1. Physical and mineralogical methods*, American Society of Agronomy, Madison, WI, 443-450.

Fisk W. J., Modera M. P., Sextro R. G., Garbesi K., Wollenberg H. A., Narasimhan T. N., Nuzum T. and Tsang Y. W. (1992) Radon entry into basements: approach, experimental structures, and instrumentation of the small structures project. LBL-31864, Lawrence Berkeley National Laboratory, Berkeley CA 94720.

Flexser S., Wollenberg H. A. and Smith A. R. (1993) Distribution of radon sources and effects on radon emanation in granitic soil at Ben Lomond, California. *Environ. Geol.* **22**, 162-177.

Fukuda H. (1955) Air and vapor movement in soil due to wind gustiness. *Soil Science* **4**, 249-256.

Garbesi K., Sextro R. G., Fisk W. J., Modera M. P. and Revzan K. L. (1993) Soil-gas entry into an experimental basement: Model-measurement comparisons and seasonal effects. *Environ. Sci. Technol.* **27**, 466-473.

Garbesi K., Sextro R. G., Robinson A. L., Wooley J. D., Owens J. A. and Nazaroff W. W. (1995) Scale dependence of soil permeability to air: Measurement method and field investigation. LBL-35369, Lawrence Berkeley Laboratory, Berkeley CA 94720.

Gossard E. E. (1960) Spectra of atmospheric scalars. *J. Geophys. Res.* **65**, 3339-3351.

Gossard E. E. and Hooke W. H. (1975) *Waves in the atmosphere: atmospheric infrasound and gravity waves -- their generation and propagation*. Elsevier, New York.

Hatton A. P., James D. D. and Swire H. W. (1970) Combined forced and natural convection with low-speed air flow over horizontal cylinders. *Journal of Fluid Mechanics* **42**, 17-31.

Hernandez T. L., Ring J. W. and Sachs H. M. (1984) The variation of basement radon concentrations with barometric pressure. *Health Phys.* **46**, 440-445.

Hintenlang D. E. and Al-Ahmady K. K. (1992) Pressure differentials for radon entry coupled to periodic atmospheric pressure variations. *Indoor Air* **2**, 208-215.

Hodgson A. T., Garbesi K., Sextro R. G. and Daisey J. M. (1992) Soil-gas contamination and entry of volatile organic compounds into a house near a landfill. *J. Air Waste Mange. Assoc.* **42**, 277-283.

Holford D. J. (1994) RN3D: A finite element code for simulating gas flow and radon transport in variably saturated, nonisothermal porous media: user's manual, version 1.0. PNL-8943, Pacific Northwest Laboratory, Richland WA 99352.

Holub R. F., Droullard R. F., Borak T. B., Inkret W. C., Morse J. G. and Baxter J. F. (1985) Radon-222 and ^{222}Rn progeny concentrations measured in an energy-efficient house equipped with a heat exchanger. *Health Phys.* **49**, 267-277.

Little J. C., Daisey J. M. and Nazaroff W. W. (1992) Transport of subsurface contaminants into buildings: An exposure pathway for volatile organics. *Environ. Sci. Technol.* **26**, 2058-2066.

Massmann J. W. (1989) Applying groundwater flow models in vapor extraction system design. *J. Environ. Eng.* **115**, 129-149.

Narasimhan T. N., Tsang Y. W. and Holman H. Y. (1990) On the potential importance of transient air flow in advective radon entry into buildings. *Geophysical Research Letters* **17**, 821-824.

Nazaroff W. W. (1992) Radon transport from soil to air. *Review of Geophysics* **30**, 137-160.

Nazaroff W. W., Moed B. A. and Sextro R. G. (1988) Soil as a source of indoor radon: Generation, migration, and entry. In Nazaroff W. W. and Nero A. V. (Ed.) *Radon and Its Decay Products in Indoor Air*, John Wiley and Sons, New York, 57-112.

Neeper D. A. and Limback S. P. (1994) Frequency domain analysis of subsurface barometric flows. *EOS, Transactions, American Geophysical Union 1994 Fall Meeting* **75**,

Nilson R. H., Peterson E. W., Lie K. H., Burkhard N. R. and Hearst J. R. (1991) Atmospheric pumping: A mechanism causing vertical transport of contaminated gases through fractured permeable media. *J. Geophys. Res.* **96**, 21933-21948.

Robinson A. L. and Sextro R. G. (1995a) Direct measurements of soil-gas entry into an experimental basement driven by atmospheric pressure fluctuations. *Geophysical Research Letters* **22**, 1929-1932.

Robinson A. L. and Sextro R. G. (1995b) The influence of a subslab gravel layer and open area on soil-gas and radon entry into two experimental basements. *Health Phys.* **69**, 367-377.

Robinson A. L., Sextro R. G. and Riley W. J. (1996) Soil-gas entry into houses driven by atmospheric pressure fluctuations, part 2 --- The influence of soil properties. LBL-38233, Lawrence Berkeley Laboratory, Berkeley CA 94720.

Scott A. G. (1988) Preventing radon entry. In Nazaroff W. W. and Nero A. V. (Ed.) *Radon and Its Decay Products in Indoor Air*, John Wiley and Sons, New York, N.Y., 407-433.

Tsang Y. W. and Narasimhan T. N. (1992) Effects of periodic atmospheric pressure variation on radon entry into buildings. *J. Geophys. Res.* **97**, 9161-9170.

Turk B. H., Prill R. J., Sextro R. G. and Harrison J. (1989) Intensive radon mitigation research: lessons learned. The 1988 International Symposium on Radon and Radon Reduction Technology. U.S. Environmental Protection Agency, Air and Energy Environmental Research Laboratory, Research Triangle Park NC 27711.

Weeks E. P. (1979) Barometric fluctuations in wells tapping deep unconfined aquifers. *Wat. Resour. Res.* **15**, 1167-1176.

Wood J. A. and Porter M. L. (1987) Hazardous pollutants in class II landfills. *J. Air. Pollut. Control Assoc.* **37**, 609-615.

NOMENCLATURE

A	Vertical cross-sectional area of structure gravel layer (m^2)
arg( )	Argument of a complex number (-)
$d\chi(\omega)$	Frequency response function defined by eqn. (6a) ($m^3\ s^{-1}\ Pa^{-1}$)
D_p	Pressure diffusivity of soil defined by eqn. (2) ($m^2\ s^{-1}$)
f_{dp}	Time-rate-of-change of atmospheric pressure power spectrum ($Pa^2\ s^{-1}$)
f_p	Atmospheric pressure power spectrum (Pa^2 s)
f_q	Soil-gas flow power spectrum ($m^6\ s^{-1}$)
g	Acceleration of gravity (9.8 m s^{-2})
$G_{q,dp}(\omega)$	Gain function, amplitude of q(t) caused by a 1 Pa s^{-1} oscillation in the time-rate-of-change in atmospheric pressure ($m^3\ Pa^{-1}$)
$G_{q,p}(\omega)$	Gain function, amplitude of q(t) caused by a 1 Pa oscillation in atmospheric pressure ($m^3\ s^{-1}\ Pa^{-1}$)
i	$\sqrt{-1}$
k	Soil permeability to gas flow (m^2)
L	Vertical distance between bottom of gravel layer and water table (m)
n	Summation index (-)
p	Soil-gas pressure (Pa)
$\overline{P}$	Mean soil-gas pressure (Pa)
P1	Prescribed pressure boundary condition at soil surface (Pa)
P2	Prescribed pressure boundary condition at the mouth of the hole in structure floor (Pa)
$P_{atm}(t)$	Atmospheric pressure (Pa)
$P'_{atm}(t)$	Time derivative of atmospheric pressure (Pa)
$q(t)$	Gas flow rate into and out of the structure in response to changes in atmospheric pressure ($m^3\ s^{-1}$)
$Q_{step}(t)$	Step response function, soil-gas flow into structure caused by a 1 Pa step change in atmospheric pressure ($m^3\ s^{-1}\ Pa^{-1}$)
$Q'_{step}(t)$	Time derivative of step response function ($m^3\ s^{-2}\ Pa^{-1}$)
r	Radial coordinate (m)
t	Time (s)
T_n	Time for index n (s)
$\overline{v}$	Soil-gas velocity vector (m s^{-1})
z	Vertical coordinate (m)
$\chi(\omega)$	Frequency response function defined by eqn. (6a) ($m^3\ Pa^{-1}$)
$\chi_a(\omega)$	Frequency response function defined by analytical model defined by eqn. (10) ($m^3\ Pa^{-1}$)
ε	Air-filled porosity (-)
$\phi_{q,dp}(\omega)$	Phase function, phase shift between q(t) and oscillations in the time-rate-of-change of atmospheric pressure (radians)
$\phi_{q,p}(\omega)$	Phase function, phase shift between q(t) and oscillations in atmospheric pressure (radians)
μ	Dynamic viscosity of soil-gas (Pa s)
θ	Dummy variable used to integrate over time (s)
τ	Characteristic response time of soil-structure system to a change in atmospheric pressure (s)
ω	Circular frequency (radians s^{-1})
$\lvert\ \rvert$	Modulus of a complex number (-)

Table 1. Measured soil and gravel permeability at the structure site used as inputs for numerical simulations.

Soil Region	Permeability (m^2)
undisturbed[a]	3.0×10^{-11} (h) ; 1.8×10^{-11} (v)
backfill[b]	3.5×10^{-12}
gravel[c]	2.0×10^{-8}

[a] Horizontal permeability (h) based on measured permeability at 3.5-m length scale; vertical permeability (v) based on measured ratio of vertical to horizontal permeability (Garbesi *et al.*, 1995).

[b] The average of single-point measurements taken around the basement structure (Garbesi *et al.*, 1993).

[c] Based on laboratory measurements in a vertical column filled with a sample of the gravel used below the basement structure (Fisk *et al.*, 1992)

Table 2. Measured air-filled porosity of the soil at the structure site used for numerical simulations.

Depth of layer (m)	ε, Air-filled porosity
0.0 - 1.6[a]	0.45
1.6 - 2.2[a]	Approximately linear decrease from 0.45 to 0.25
2.2 - 5.0[a]	0.25
5.0 - 8.5[b]	0.25 (inferred)

[a] Based on gravimetric analysis (Danielson and Sutherland, 1986) of soil cores taken by Flexser *et al.* (1993).

[b] We have extended the measured profile to 8.5 m, the measured depth of the water table below the soil surface.

Table 3. Soil and geometric properties used as inputs for the analytical model.

Property	Value
Soil permeability to air, k	3×10^{-11} m^2
Air-filled porosity of the soil, ε	0.40
Mean soil-gas pressure, $\overline{P}$	92 kPa
Dynamic viscosity of soil gas, μ	1.8×10^{-5} Pa s
Pressure diffusivity, D_p	0.39 m^2 s^{-1}
Vertical cross-sectional area of gravel layer, A	5 m^2
Water table depth below structure, L	6.5 m

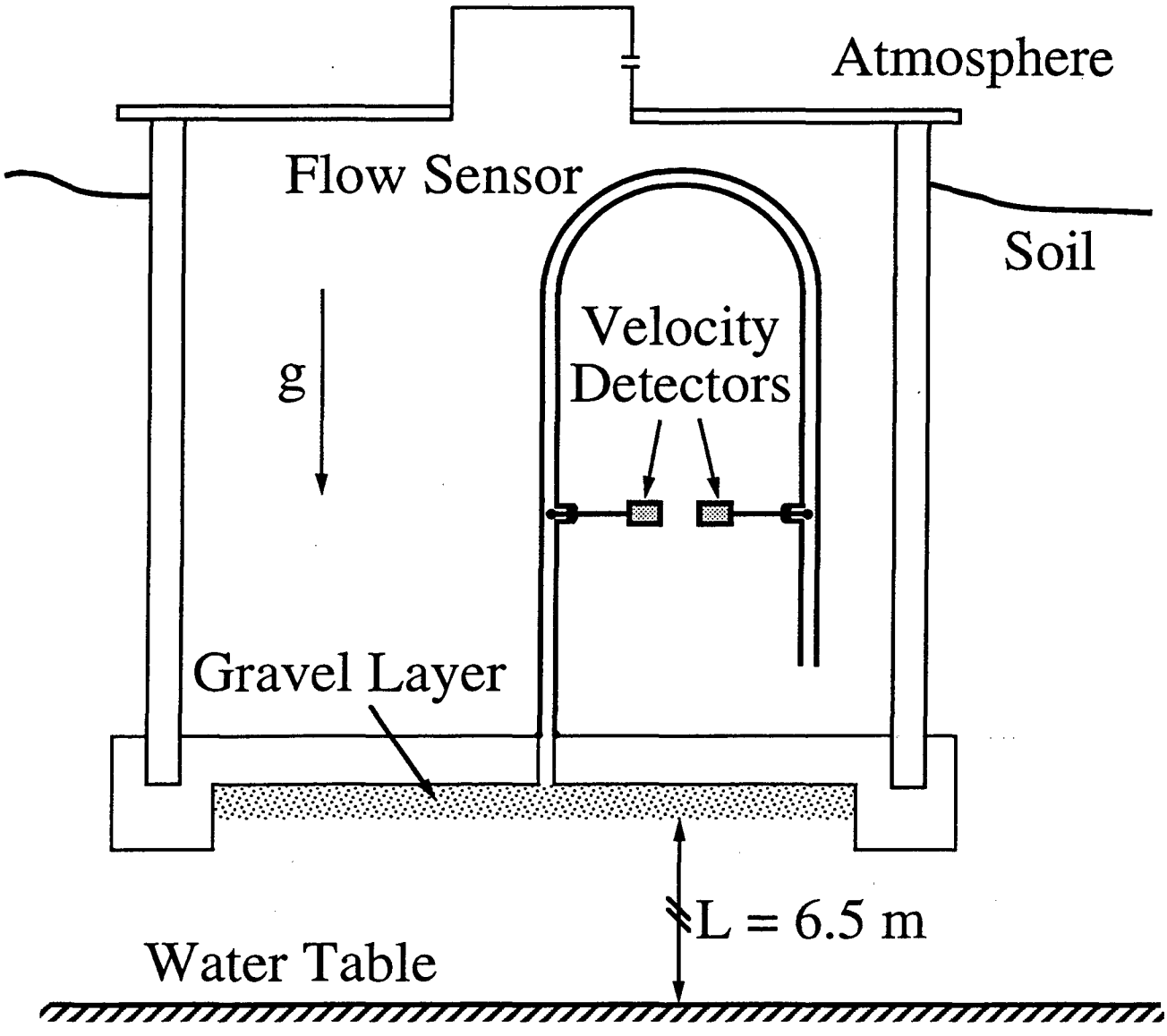

Fig. 1 Schematic of experimental structure and flow sensor. The figure is not drawn to-scale.

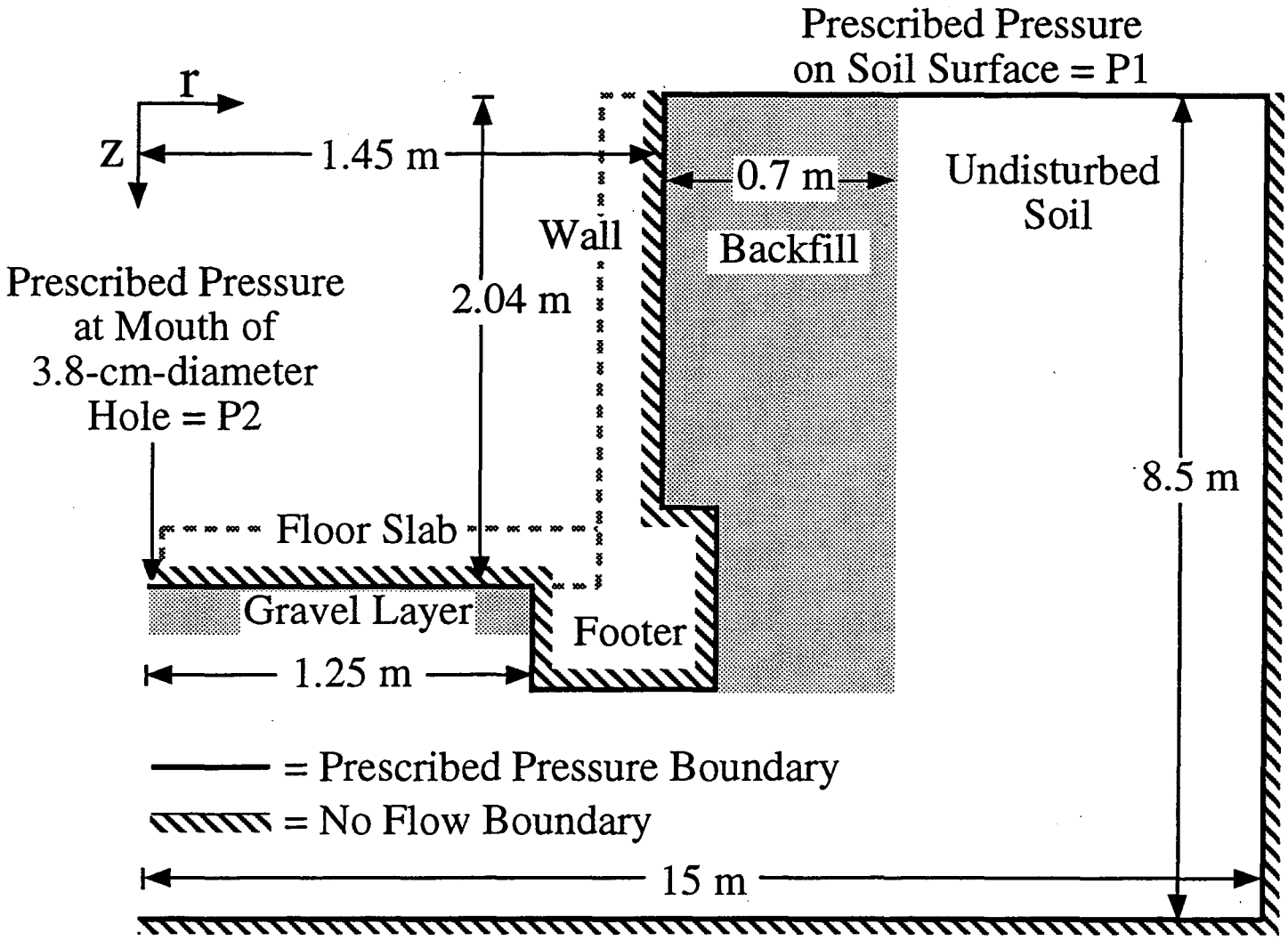

Fig. 2 Schematic of cylindrical structure and soil block simulated by finite-element model. Due to the axial-symmetry only half of the cylinder is shown. The finite-element model calculates the soil-gas pressure and velocity inside the region bound by the heavy black line. The dashed lines indicate the interior edge of the walls of the structure. These lines are intended for visual guidance only. The figure is not drawn to scale.

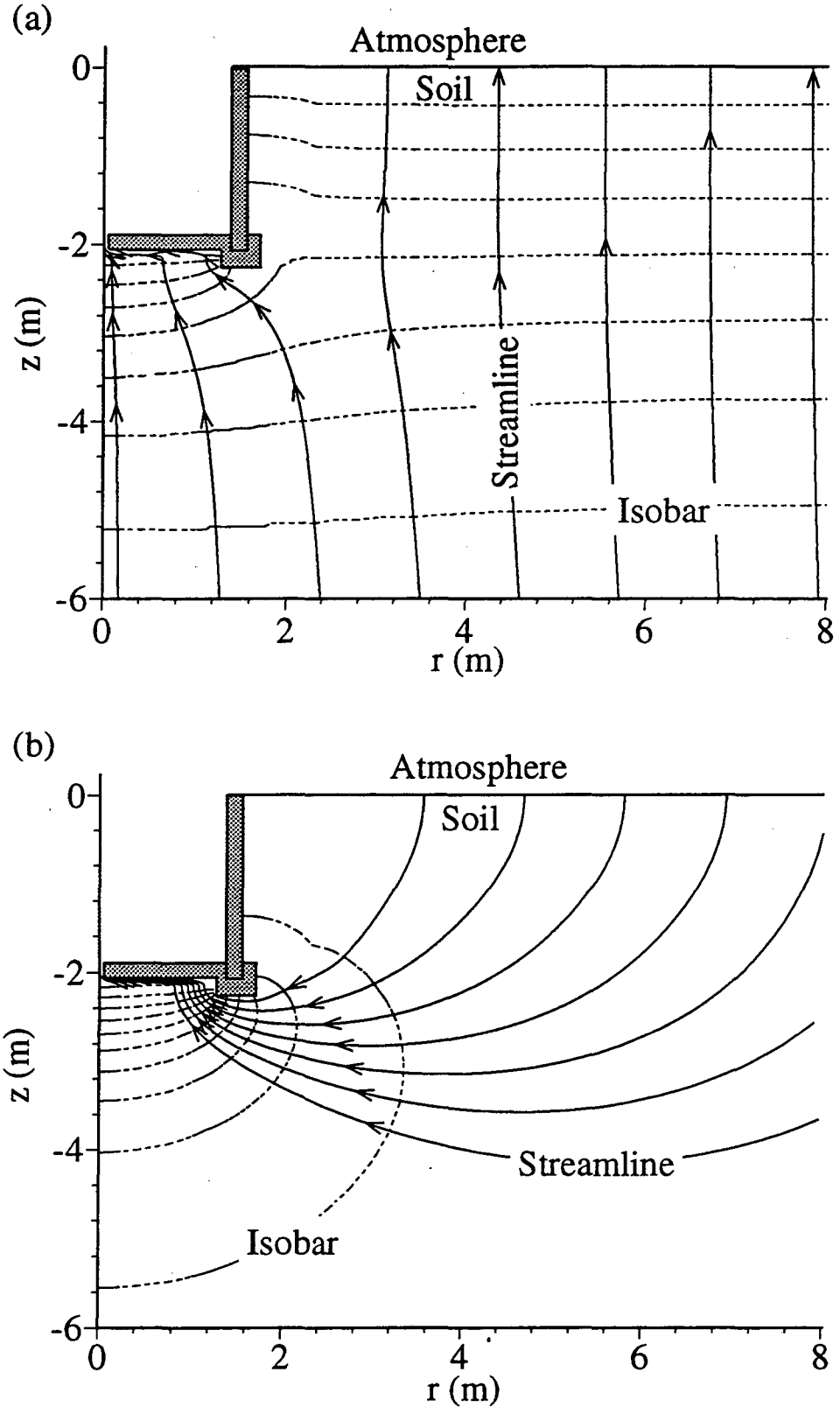

Fig. 3 Calculated soil-gas velocity and pressure fields: (a) caused by a constant negative time-rate-of-change in atmospheric pressure; (b) caused by a steady indoor-outdoor pressure difference. Solid lines indicate streamlines, and dashed lines indicate isobars. Soil-gas pressures have been corrected for hydrostatic effects to illustrate the pressure gradients which drive the flow.

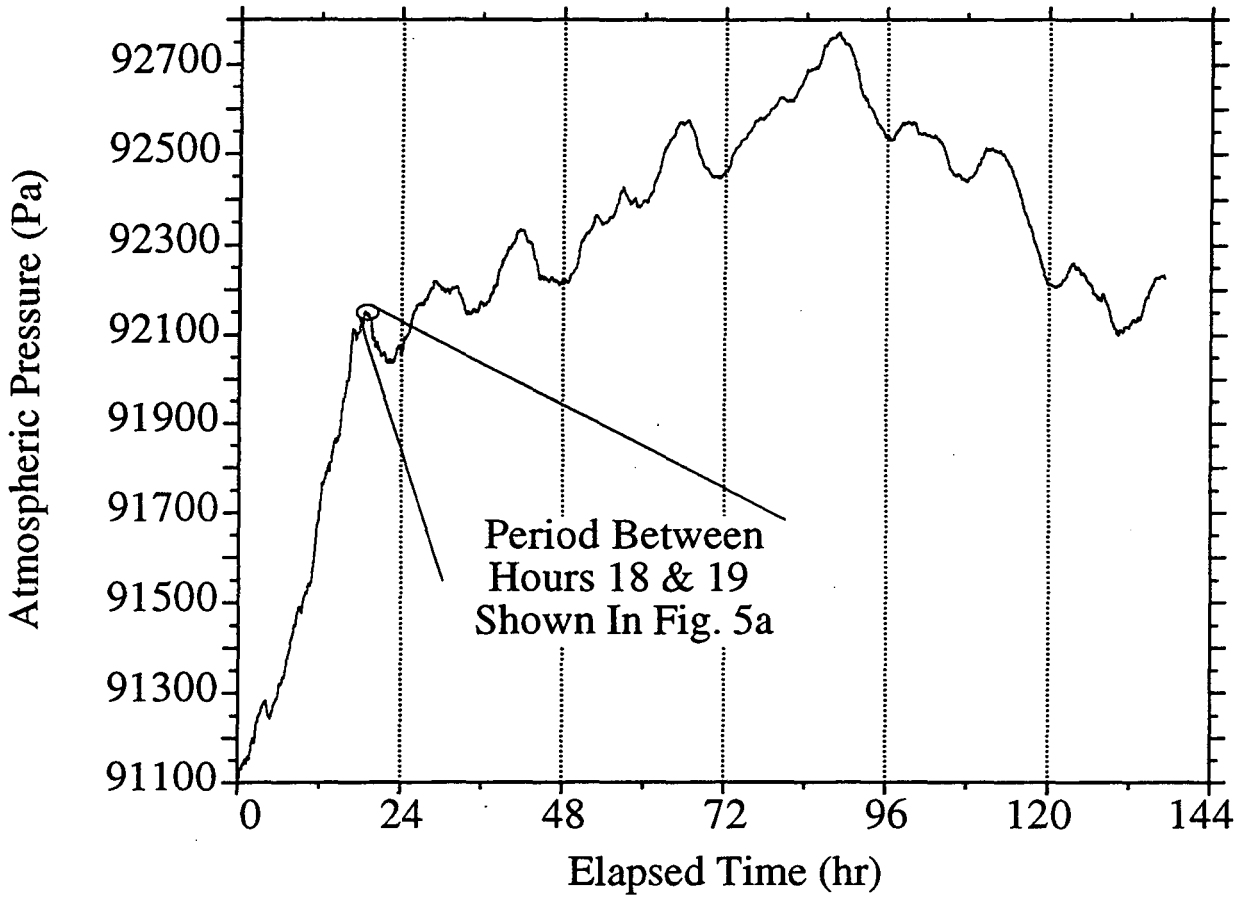

Fig. 4 Atmospheric pressure measured during a six-day experiment conducted in the fall of 1994. Between hours 0 and 16 a passing weather front caused a 1000 Pa change in atmospheric pressure.

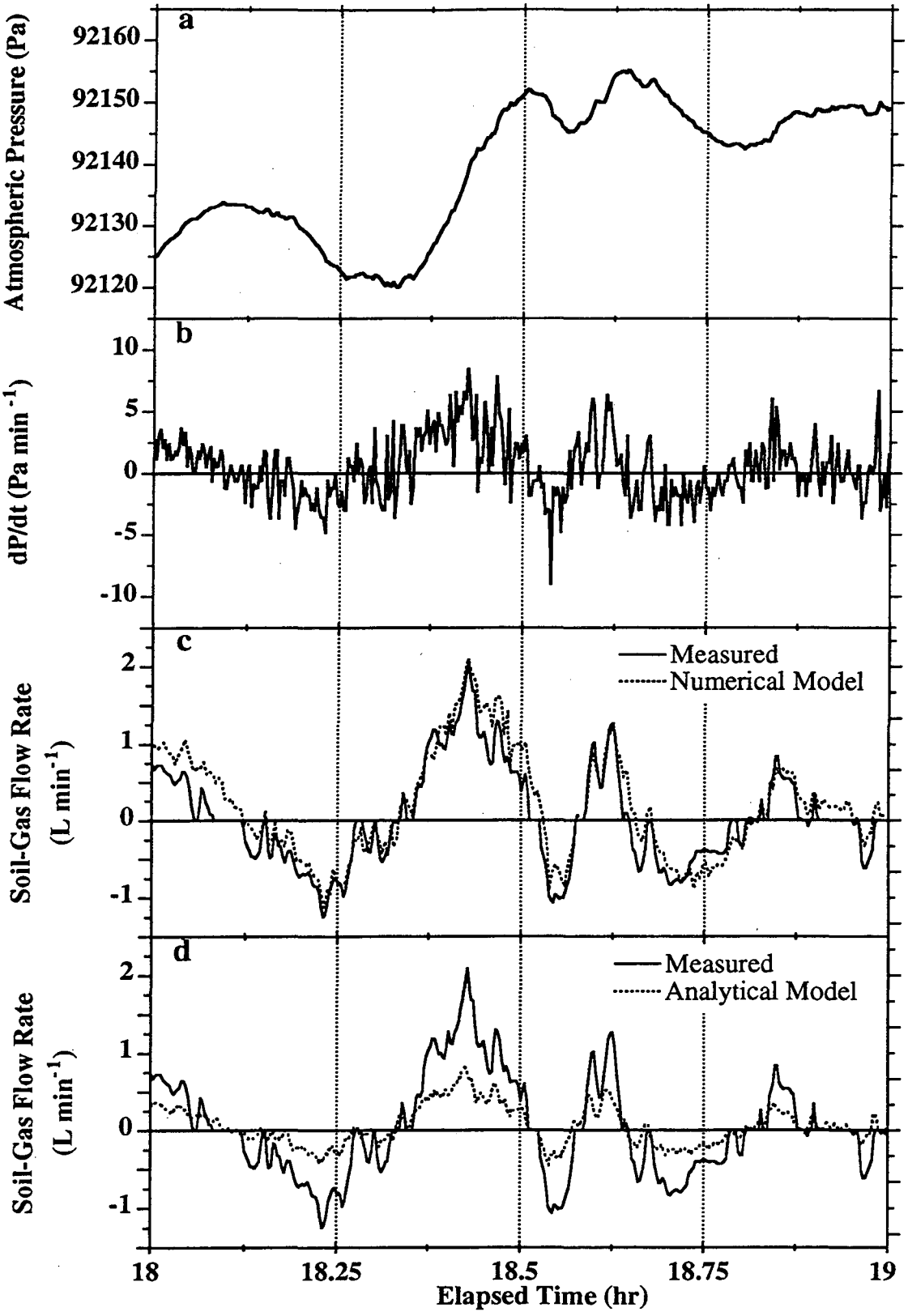

Fig. 5 Atmospheric pressure and the response of soil-structure system between hours 18 and 19 of the six-day experiment shown in Fig. 4: (a) measured atmospheric pressure; (b) time-rate-of-change of atmospheric pressure; (c) soil-gas flow rate (measured data represented by solid line, predictions of the numerical model shown by the dotted line); (d) soil-gas flow rate (measured data indicated by the solid line, predictions of the analytical model shown by the dotted line). Negative soil-gas flow indicates flow into the experimental structure. Uncertainty of the measured soil-gas flow rates is less than 5%.

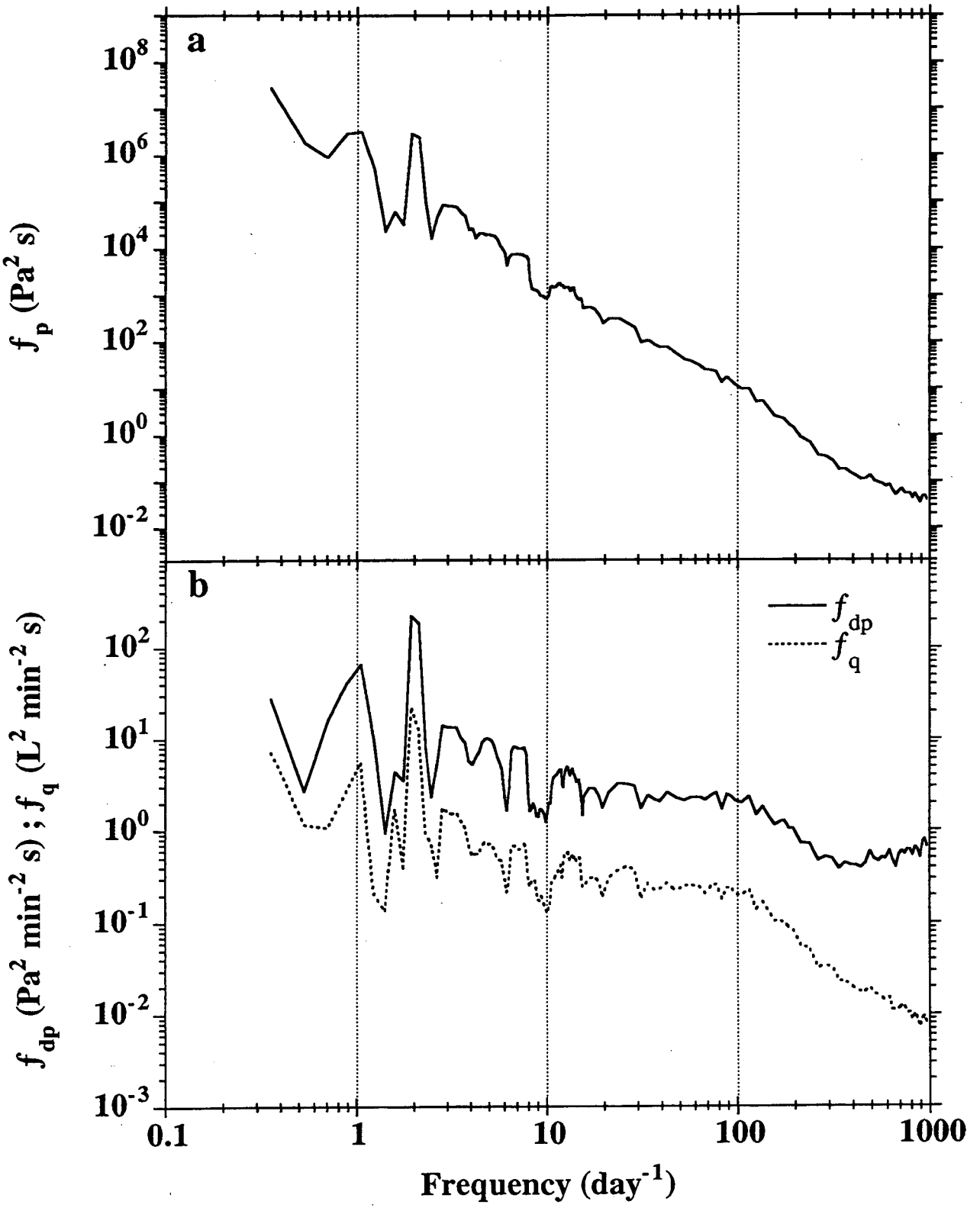

Fig. 6 Smoothed power spectra estimated from 21 days of experimental data: (a) f_p, atmospheric pressure; (b) f_{dp}, time-rate-of-change of atmospheric pressure, and f_q, soil-gas entry rate.

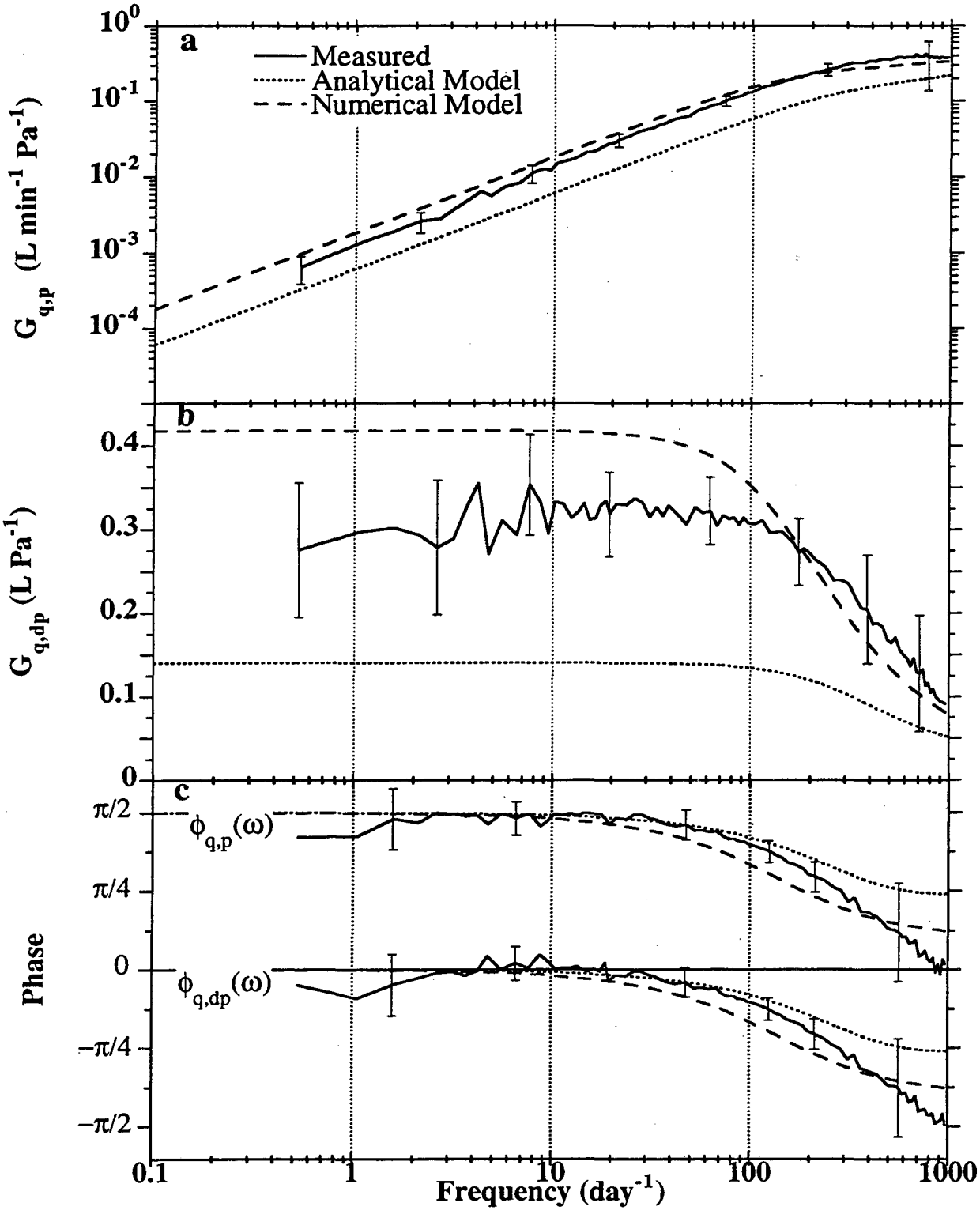

Fig. 7 Measured and predicted gain and phase functions: (a) $G_{q,p}(\omega)$, amplitude of the soil-gas entry rate caused by a 1 Pa oscillation in atmospheric pressure; (b) $G_{q,dp}(\omega)$, amplitude of the soil-gas entry rate caused by 1 Pa min^{-1} oscillation in the time-rate-of-change of atmospheric pressure; (c) $\phi_{q,p}(\omega)$, phase lag between the soil-gas entry rate and an oscillation in atmospheric pressure; $\phi_{q,dp}(\omega)$, phase lag between the soil-gas entry rate and an oscillation in the time-rate-of-change of atmospheric pressure. Vertical bars indicate measurement uncertainty.

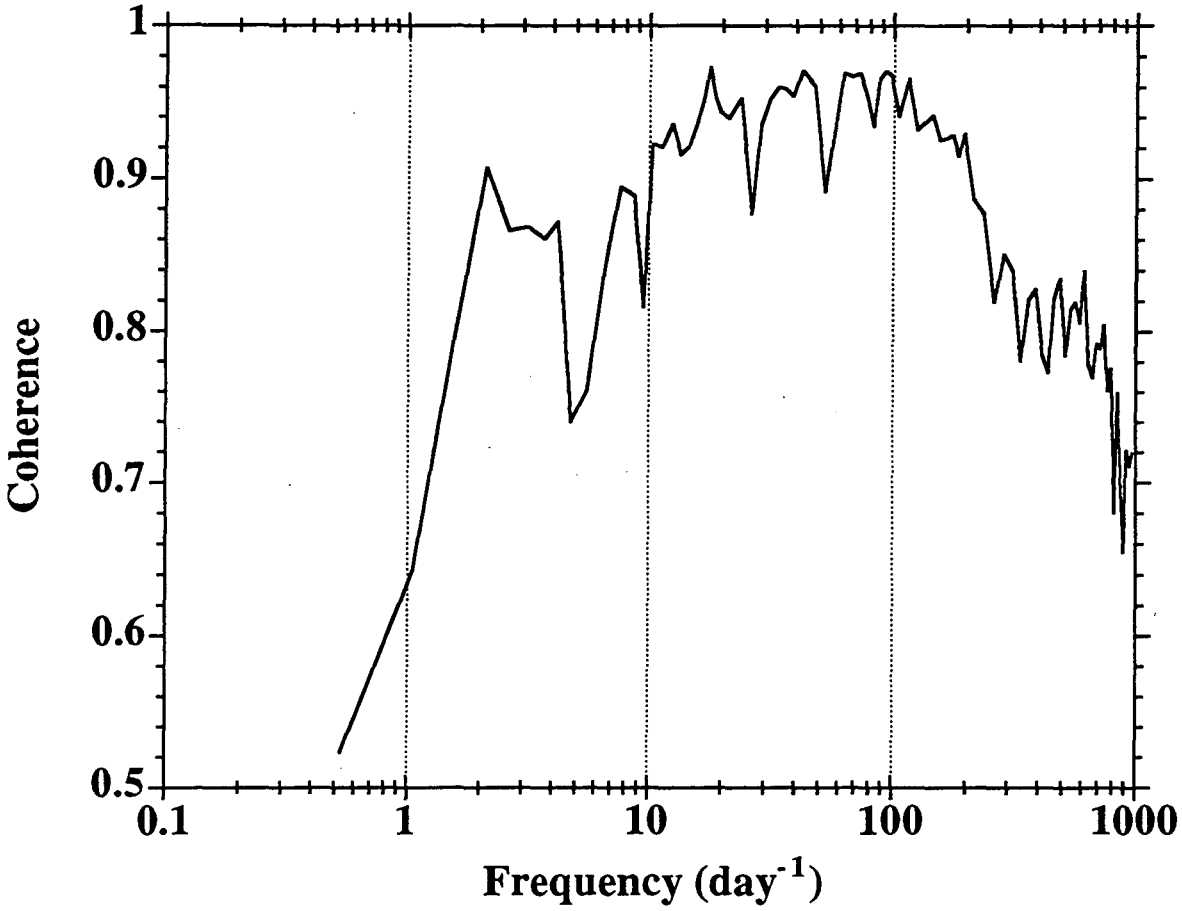

Fig. 8 Coherence between measured soil-gas flow and changes in atmospheric pressure.

LAWRENCE BERKELEY NATIONAL LABORATORY
UNIVERSITY OF CALIFORNIA
TECHNICAL & ELECTRONIC INFORMATION DEPARTMENT
BERKELEY, CALIFORNIA 94720